

















Time-resolved Auger–Meitner spectroscopy of the photodissociation dynamics of CS₂

Henry J Thompson¹ , Oksana Plekan² , Matteo Bonanomi^{3,5}, Nitish Pal² , Felix Allum⁹ , Alexander D Brynes² , Marcello Coreno⁶, Sonia Coriani¹⁴, Miltcho B Danailov², Piero Decleva^{4,11} , Alexander Demidovich², Michele Devetta⁵ , Davide Faccialà⁵ , Raimund Feifel⁷, Ruaridh Forbes⁹ , Cesare Grazioli⁴ , David M P Holland⁸ , Paolo Piseri³, Kevin C Prince², Daniel Rolles¹⁰ , Michael S Schuurman^{12,13}, Alberto Simoncig², Richard J Squibb⁷, Bruno N C Tenorio¹⁵, Caterina Vozzi⁵ , Marco Zangrando^{2,4}, Carlo Callegari² , Russell S Minns^{1,*}  and Michele Di Fraia^{2,4,*} 

¹ School of Chemistry, University of Southampton, Southampton SO17 1BJ, United Kingdom

² Elettra—Sincrotrone Trieste S.C.p.A., 34149 Basovizza, Italy

³ Politecnico di Milano, 20133 Milano, Italy

⁴ CNR-IOM—Istituto Officina dei Materiali, National Research Council of Italy, 34149 Trieste, Italy

⁵ CNR-IFN—Istituto di Fotonica e Nanotecnologie, National Research Council of Italy, 20133 Milano, Italy

⁶ CNR-ISM—Istituto Struttura della Materia, National Research Council of Italy, 34149 Trieste, Italy

⁷ Department of Physics, University of Gothenburg, SE-412 96 Gothenburg, Sweden

⁸ STFC, Daresbury Laboratory, Warrington WA4 4AD, United Kingdom

⁹ Linac Coherent Light Source, SLAC National Accelerator Laboratory, Menlo Park 94025 CA, United States of America

¹⁰ J.R. Macdonald Laboratory, Department of Physics, Kansas State University, Manhattan 66506 KS, United States of America

¹¹ Dipartimento di Scienze Chimiche e Farmaceutiche, Università degli Studi di Trieste, I-34121 Trieste, Italy

¹² National Research Council of Canada, Ottawa, ON, Canada

¹³ Department of Chemistry and Biomolecular Sciences, University of Ottawa, Ottawa, ON, Canada

¹⁴ Department of Chemistry, Technical University of Denmark, DK-2800 Kgs. Lyngby, Denmark

¹⁵ Instituto Madrileño de Estudios Avanzados en Nanociencia (IMDEA-Nanociencia), 28049 Madrid, Spain

E-mail: r.s.minns@soton.ac.uk and difraia@iom.cnr.it

Received 26 June 2024, revised 13 August 2024

Accepted for publication 10 September 2024

Published 1 October 2024



CrossMark

Abstract

The photodissociation dynamics of UV excited CS₂ are investigated using time-resolved Auger–Meitner (AM) spectroscopy. AM decay is initiated by inner-shell ionisation with a femtosecond duration x-ray (179.9 eV) probe generated by the FERMI free electron laser. The time-delayed x-ray probe removes an electron from the S(2p) orbital leading to secondary emission of a high energy electron through AM decay. We monitor the electron kinetic energy

* Authors to whom any correspondence should be addressed.



Original Content from this work may be used under the terms of the [Creative Commons Attribution 4.0 licence](https://creativecommons.org/licenses/by/4.0/). Any further distribution of this work must maintain attribution to the author(s) and the title of the work, journal citation and DOI.

of the AM emission as a function of pump-probe delay and observe time-dependent changes in the spectrum that correlate with the formation of bound, excited-state CS₂ molecules at early times, and CS + S fragments on the picosecond timescale. The results are analysed based on a simplified kinetic scheme that provides a time constant for dissociation of approximately 1.2 ps, in agreement with previous time-resolved x-ray photoelectron spectroscopy measurements (Gabalski, *et al* 2023 *J. Phys. Chem. Lett.* **14** 7126–7133).

Keywords: Auger spectroscopy, free electron lasers, time-resolved x-ray spectroscopy

1. Introduction

The photodissociation dynamics of CS₂ involve competing internal conversion (IC) and intersystem crossing (ISC) processes, that are coupled to structural changes that result in the molecule bending and asymmetrically stretching. The overall dynamics lead to the formation of ground state CS and atomic S in either the ground (³P) or spin-orbit excited (¹D) state (Hemley *et al* 1983, Waller and Hepburn 1987, Mank *et al* 1996, Farmanara *et al* 1999, Townsend *et al* 2006, Bisgaard *et al* 2009, Hockett *et al* 2011, Brouard *et al* 2012). This complex interplay of nuclear and electronic degrees of freedom means that the photodissociation dynamics of CS₂ stand as a benchmark system for the study of complex photochemical processes in a structurally simple system, leading to its position as a molecule of choice when testing and developing new experimental probes (Bisgaard *et al* 2009, Horio *et al* 2013, 2017, Spesyvtsev *et al* 2015, Smith *et al* 2018, Karashima *et al* 2021, Warne *et al* 2021, Gabalski *et al* 2022, 2023, Razmus *et al* 2022, Unwin *et al* 2023).

The static investigation of molecules at the core, by means of x-ray photoelectron spectroscopy (XPS) and Auger spectroscopy, with synchrotron radiation is a well-established field of research, capable of providing detailed information (Ankerhold *et al* 1997, Bolognesi *et al* 2009, Hedin *et al* 2009, Sekushin *et al* 2012, Hikosaka *et al* 2014). With the advent of free electron laser (FEL) technology and the accessibility of femtosecond duration X-ray pulses, measurements have sought to exploit the element specificity of X-ray probes to explore the sensitivity of more strongly bound (core) electrons to photochemical change. Of most relevance to the present study are recent experiments that use time-resolved XPS probes that either measure the primary photoemission (Brauß *et al* 2018, Mayer *et al* 2022, Gabalski *et al* 2023) or secondary processes such as Auger–Meitner (AM) emission (McFarland *et al* 2014, Lever *et al* 2020, Wolf *et al* 2021) to probe photochemical change.

Schematic representations of both XPS and AM processes are provided in figure 1 and can be described as follows. In the electronic ground state (top left panel), x-ray ionisation removes a core electron and leaves the molecule in an unstable electronic configuration. Subsequent relaxation leads to an electron in a higher lying orbital making a transition to fill the core vacancy, with the excess energy taken away through the emission of a secondary electron with a typical timescale of a few femtoseconds. Radiative processes like fluorescence are generally competing with AM processes but are very weak

at the specific sulfur L-subshells considered in this manuscript, and thus neglected in this representation (Krause 1979). Figure 1 shows one of many AM transitions that are possible, leading to an often complex spectrum that shows sensitivity to both core and valence electronic structure. In the time-resolved variant (bottom panel), UV excitation leads to a change in the valence electronic structure such that, following X-ray ionisation, the subsequent AM decay process may also differ from those in the unexcited molecule. Following the initial excitation, the electronic and geometric structure of the molecule evolves over time, within tens or hundreds of femtoseconds, leading to changes in the observed AM spectrum. A potential advantage of time-resolved AM spectroscopy (TR-AMS) methods is that the energy of the AM emission is controlled by the molecular electronic structure and is independent of the ionising photon energy.

Previous TR-AMS measurements have been used to study the non-adiabatic processes involved in the photochemical relaxation of thymine (McFarland *et al* 2014) and two-thiouracil (Lever *et al* 2020). Analysis of the electron peak intensities, and the way in which the peaks shift with pump-probe delay were interpreted in terms of electronic and geometric structure changes. Electronic structure changes in thymine led to new bands appearing in the oxygen K-edge AM spectrum, while C-S bond extensions occurring in two-thiouracil led to characteristic shifts in the S(2p) AM spectrum with subsequent electronic state changes leading to shifts in the band positions over much longer timescales. We note that AM processes can also be initiated by non-ionising transitions from core to unoccupied valence states. In the resonant case, the potential advantage of the emission being independent of the x-ray energy is lost. However, the location of the resonant transition can provide extra information about the character of the valence hole created upon UV excitation (Wolf *et al* 2021). In recent resonant TR-AMS experiments of thymine (Wolf *et al* 2021), measurements were able to identify the evolving character of the excited thymine molecule, characterising the ISC between singlet and triplet $\pi\pi^*$ states.

Returning to the study of CS₂, a recent time-resolved XPS (TR-XPS) measurement investigated the UV driven photodissociation reactions of CS₂ (Gabalski *et al* 2023). The measurements were performed at the sulfur 2p edge and showed large shifts in the photoelectron bands associated with the excited states and dissociation products. The relatively broad effective bandwidth of the SASE (self-amplified spontaneous emission) FEL output however limited the attainable spectral resolution. Herein we report on a complementary TR-AMS

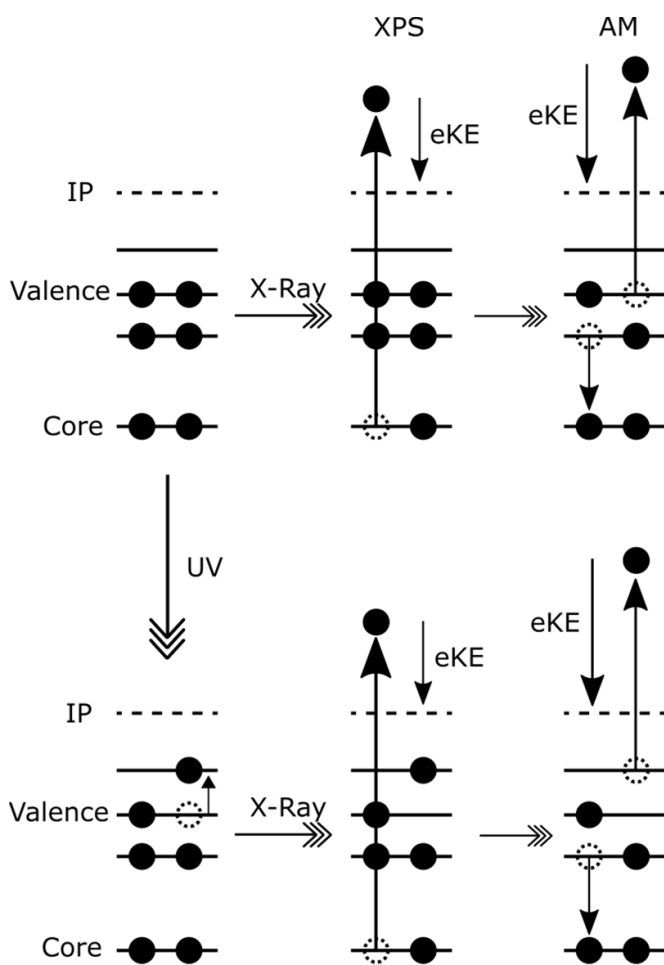


Figure 1. Schematic representation of the AM process in both ground (top) and UV excited (bottom) states. In both the electronic ground and the UV excited states, x-ray ionisation removes a core electron leaving the molecular ion in an unstable electronic configuration. Subsequent relaxation leads to a transition of an electron in a higher lying orbital filling the core hole, with the excess energy taken away through the emission of an AM electron. As the valence structures of the ground and UV excited molecules are different, the measured electron kinetic energies in the AM spectrum will reflect the change in the valence electronic structure.

study to examine the time-dependent changes in the AM emission following ionisation of the S(2p) orbital of UV excited CS₂. In the experiments, the absorption of a 6.2 eV (200 nm) photon electronically excites CS₂ leading to C-S bond fission and the eventual formation of CS and S fragments. The UV excited molecule is ionised through the absorption of a 179.9 eV photon to remove a S(2p) electron, resulting in AM emission. Time-dependent changes in the AM spectrum allow us to monitor the changes in electronic character associated with excitation and dissociation of CS₂ following UV excitation.

2. Experimental details

The experiment has been performed at the low density matter (LDM) beamline (Svetina *et al* 2015) of the seeded FEL

FERMI (Allaria *et al* 2015) in Trieste (Italy). The basic layout of the endstation described in Lyamayev *et al* (2013) does not include the magnetic bottle electron spectrometer (MBES), which became available as a later upgrade (Squibb *et al* 2018) and was the configuration of choice in the present experiment, with the axis of the MBES oriented vertically. A retardation voltage was applied to the time-of-flight tube to slow down the AM electrons and thus improve the spectral resolution. The retardation voltage was 100 V which effectively rejects any electrons with an energy lower than 100 eV and reduces the energy of all electrons above this energy by 100 eV. All of the plots presented in the manuscript have been corrected for this retardation voltage and therefore represent the kinetic energy of the electron following photoionisation which is 100 eV higher than the energy measured.

The pump laser setup is based on the availability of IR pulses from the Titanium-Sapphire (Ti:Sa) laser that drives the FERMI seed system (Cinquegrana *et al* 2021); the pulses are sent to an optical table attached to the endstation where they are further conditioned (intensity, polarisation, focus translation, delay, harmonic upconversion). The basic layout of this system (conventionally: SLU, Seed Laser for Users) is described in Finetti *et al* (2017); it has been meanwhile upgraded to include fourth harmonic generation (via sequential second-harmonic generation and sum-frequency generation) with the following parameters: central wavelength 199.72 nm; bandwidth 0.86 nm (FWHM); pulse duration 160 fs (FWHM); 50 Hz repetition rate (optionally downsampled). Up to 5 μ J of light can be generated, greatly exceeding the needs of the experiment (measurements were done at 0.2 μ J, by reducing the intensity of the input IR). The absorption spectrum of CS₂ measured by Hemley *et al* (1983) suggests that the transitions excited by the SLU originate mainly from the vibrationally unexcited ground state, but with a small contribution from the level having one quantum of the bending mode. The upper levels populated will contain several quanta in the symmetric stretching and/or bending vibrational modes.

The FEL probe pulse is generated in the FEL-2 machine (Allaria *et al* 2013), set to produce harmonic 12 of a 248 nm seed in the first stage, and harmonic 3 of the resulting 20.67 nm pulse (6.89 nm) in the second stage; metal foil filters are available along the photon transport line to alter the balance of the two pulses, in particular to abate the first-stage pulse. The FEL pulse duration was estimated to be about 30 fs. Long-term stable overlap is maintained by active trajectory feedback systems. The SLU repetition rate was set to 25 Hz, which is half of the FEL repetition rate. This allows alternate FEL-only spectra and FEL + SLU spectra to be recorded in order to generate differential spectra in post acquisition analysis. The temporal (t_0) and spatial overlap between the FEL and SLU pulses was determined through two-colour ionisation of helium. The first stage radiation of the FEL was tuned to 52.22 nm to excite the $1s^2 \rightarrow 1s4p$ transition which was subsequently ionised by the SLU pulse.

A mixture of 0.14 bar CS₂ in 2 bar helium was expanded into vacuum with a commercial pulsed Valve (Parker Series 9, orifice aperture 250 μ m) operated at the FEL repetition rate,

50 Hz, and nominal opening time 110 μ s in the endstation's source chamber; a supersonic jet is formed along the horizontal long axis of the endstation, and passes through a conical skimmer (Beam Dynamics model 76.2, 3 mm diameter) into a differential pumping chamber, where it is further defined by a fixed-diameter iris (1.5 mm) and a set of piezoelectrically-operated vertical slits (Piezosystem Jena PZS 3) before entering the detector chamber. In the detector chamber the molecular beam perpendicularly crosses the FEL beam, the latter propagating along the horizontal short axis of the endstation. The SLU beam is sent into the detector chamber quasi-collinearly with the FEL (4° downward tilt).

A calibration of the spectrometer was achieved by changing the FEL photon energy and measuring the position of carrier gas (He) photoelectron peak. Photoelectron spectra of helium were measured at photon energies of 30, 55, 60 and 179.95 eV, without filters and for different retardation voltages.

For all of the experimental data presented the pump polarisation is perpendicular to the FEL probe polarisation, and the FEL polarisation is perpendicular to the MBES time-of-flight axis. Measurements with parallel pump and probe polarisations were also made and these showed identical time-dependent changes but with overall lower statistics.

3. Results and discussion

In figure 2 we plot the spectrum obtained from ionisation of ground state CS_2 with a FEL photon energy of 179.9 eV (6.89 nm) and bandwidth of 280 meV FWHM. The spectrum contains peaks due to ionisation of the valence orbitals at kinetic energies between 160 and 170 eV, and peaks due to AM decay at kinetic energies between 125 and 144 eV. The ionisation energies of the $\text{S } 2^2\text{P}_{3/2}$ and $2^2\text{P}_{1/2}$ states in CS_2 are 169.81 and 171.08 eV (Hedin *et al* 2009). Thus the kinetic energy of the electrons associated with the ionisation of the $\text{S}(2p)$ orbital are approximately 10 eV. Such low energy electrons are rejected by the spectrometer due to the 100 V retardation field used to improve the energy resolution of the high kinetic energy AM electrons. Measurements of the time-resolved XPS have also been performed and will be reported as part of a future manuscript.

The AM spectrum measured is comparable to the high-resolution work of Hedin *et al* (2009) who recorded a similar spectrum using synchrotron radiation at 173.04 eV. Our spectrometer resolving power of $\Delta E/E \approx 50$ (corresponding to a kinetic energy resolution of 0.7 eV, after retardation) is comparable to, or slightly higher than, the separation between the Auger peaks, resulting in the broad bands observed in both the valence and AM regions of the spectrum. We therefore do not provide a detailed analysis of the peaks, and refer the reader to the work of Hedin *et al* (2009) for a more detailed discussion of the underlying transitions.

In figure 3 we present differential time-resolved photoelectron spectra encompassing the high kinetic energy valence photoelectrons, collected at the same time as the AM spectra presented later. The spectra are obtained by alternating pump-on and pump-off shots and plotting the aggregated difference

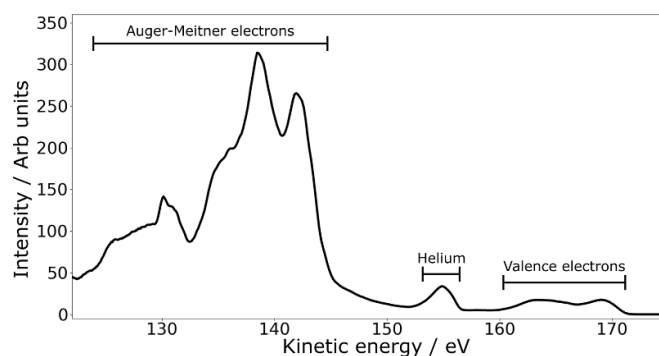


Figure 2. Electron spectrum of CS_2 obtained following ionisation with a 179.9 eV photon. Regions of the spectrum are labelled to highlight the processes responsible for the peaks observed. Between 160 and 170 eV we observe features associated with direct ionisation of the valence electronic states of CS_2 , between 125 and 144 eV we observe peaks associated with the AM electrons emitted following ionisation from the $\text{S}(2p)$ orbital. The peak at 155 eV is due to ionisation of the helium carrier gas.

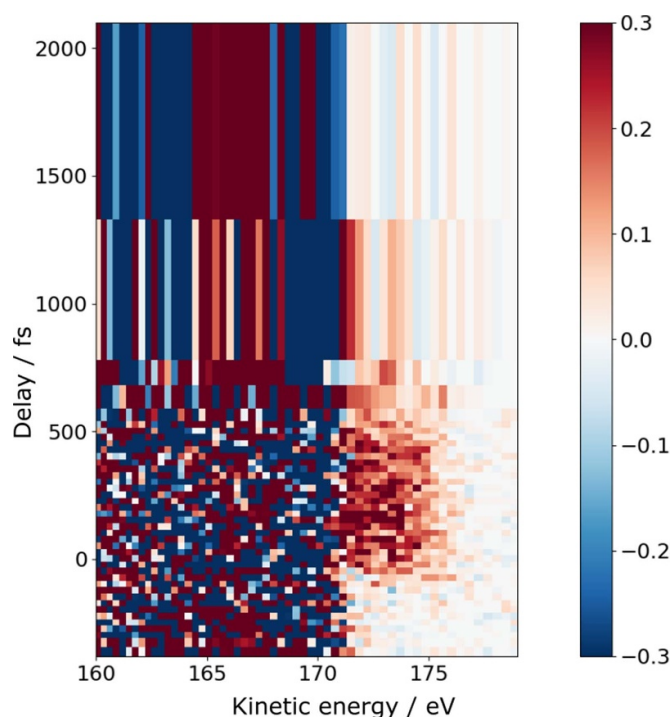


Figure 3. Differential time-resolved valence photoelectron spectrum of CS_2 following 200 nm excitation and 179.9 eV (6.89 nm) ionisation. The following delay intervals were covered: [-500 fs, +500 fs] in steps of 25 fs, [+600 fs, +800 fs] in steps of 100 fs, [+1800 fs, +3800 fs] in steps of 1 ps. These non-uniform delay steps are represented on a uniform vertical scale.

while scanning the relative pump-probe delay with variable step sizes up to 3.8 ps. The dynamics are mapped with 25 fs step size up to 500 fs and with a geometrically increasing step size from 500 fs to 3800 fs.

The difference map shows an enhanced intensity at short pump-probe delays at kinetic energies between 171.5 eV and 176 eV. This intensity is associated with electronically excited states of CS_2 . A further enhancement is observed at

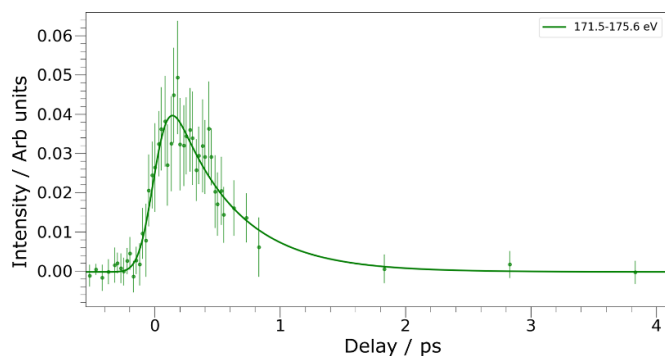


Figure 4. Integrated intensity over the electron kinetic energy range 171.5–175.6 eV (data points) and the associated fit to equation (2) (solid line). The data point errors represent twice the standard deviation confidence interval obtained through a bootstrap analysis of the integrated photoelectron yields.

large pump-probe delays at kinetic energies between 165 and 168 eV. This intensity is due to dissociation products. These observations are in line with previous valence shell photoelectron spectroscopy measurements (Smith *et al* 2018, Karashima *et al* 2021). The high kinetic energy of the presented measurement limits the spectral resolution such that a detailed analysis of the signal is not performed here. We can however use this signal to obtain an internal calibration of time-zero and of the instrument response function.

In figure 4 we plot the integrated photoelectron intensity in the kinetic energy range between 171.5 and 176 eV, associated with the electronically excited states of the bound CS₂ molecule. The data are fit to a Gaussian instrument response function convoluted with an exponential decay. The retrieved parameters provide a standard deviation of the Gaussian, $\sigma = 96.1 \pm 11.1$ fs, and an exponential time-constant, $1/\lambda = 486.1 \pm 76.1$ fs. These values are in accord with estimations obtained following off-line characterisation of the optical pulse duration, and they are also consistent with the excited state lifetime obtained in previous experiments (Smith *et al* 2018, Karashima *et al* 2021). In addition, the fit provides a calibrated time zero which is used in all plots presented in the manuscript. While we do observe the dissociation products at long time delays between 165 and 168 eV, subsequent fits of the integrated region were unsuccessful due to high levels of noise in delays prior to 500 fs. We therefore do not present a data fit of the dissociation product rise in the valence photoelectron region.

The differential AM spectra measured at pump-probe delays between -500 and 2000 fs are shown in figure 5. Around time-zero we observe a transient increase in the intensity between 140 and 148 eV and a depletion between 137 and 140 eV. The region above 144 eV is at a kinetic energy that is higher than seen in the ground state AM spectrum, see figure 2. The general shape of the early time difference AM spectrum therefore suggests the overall AM spectrum has shifted to slightly higher kinetic energies.

At delays >500 fs the character of the signal is reversed, with an increase in intensity centred around 137 eV, and

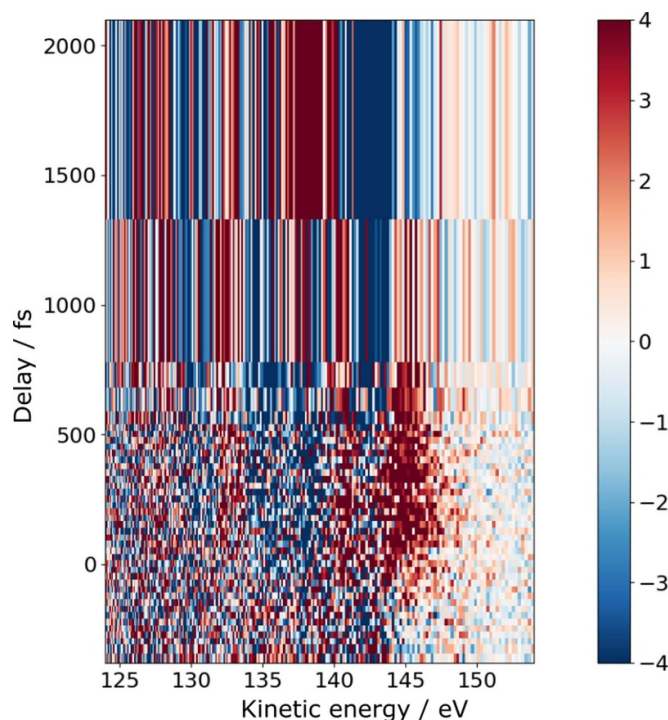


Figure 5. Differential time-resolved Auger–Meitner map of CS₂ following 200 nm excitation and 179.9 eV (6.89 nm) core ionisation. The delay is the time difference between the SLU and the FEL pulse, with negative delays indicating the FEL arriving before the SLU. The following delay intervals were covered: $[-500$ fs, $+500$ fs] in steps of 25 fs, $[+600$ fs, $+800$ fs] in steps of 100 fs, $[+1800$ fs, $+3800$ fs] in steps of 1 ps”. These non-uniform delay steps are represented on a uniform vertical scale.

a depletion centred at approximately 142 eV. The spectrum appears not to change further after delays of approximately 1 ps indicating that this relates to the final products of the dissociation reaction. The time dependent changes in the spectrum can be more clearly seen in figures 6(a)–(c) where we plot the average differential spectrum obtained over specific pump-probe delay ranges. A representative negative time (probe arrives before pump) range is plotted in panel c to provide a representation of the baseline noise level obtained in the measurements. This is compared to the average differential spectrum obtained at early (0–400 fs, b) and late (0.8–3.8 ps, a) pump-probe delays. Based on previously reported reaction timescales (Townsend *et al* 2006, Bisgaard *et al* 2009, Smith *et al* 2018, Karashima *et al* 2021) the early time spectrum should be predominantly composed of contributions relating to population in the excited states of bound CS₂, (b), while the late time spectrum will be dominated by contributions from the dissociation products, (a). The spectra show that, in line with our earlier discussion, at early times there is an increase in the higher electron kinetic energy region of the AM spectrum associated with the formation of the electronically excited states with what appears to be the formation of two peaks at 141 eV and 145 eV, figure 6(b). At late times this contribution depletes, and we observe an increase in intensity at lower electron kinetic energy associated with the formation of

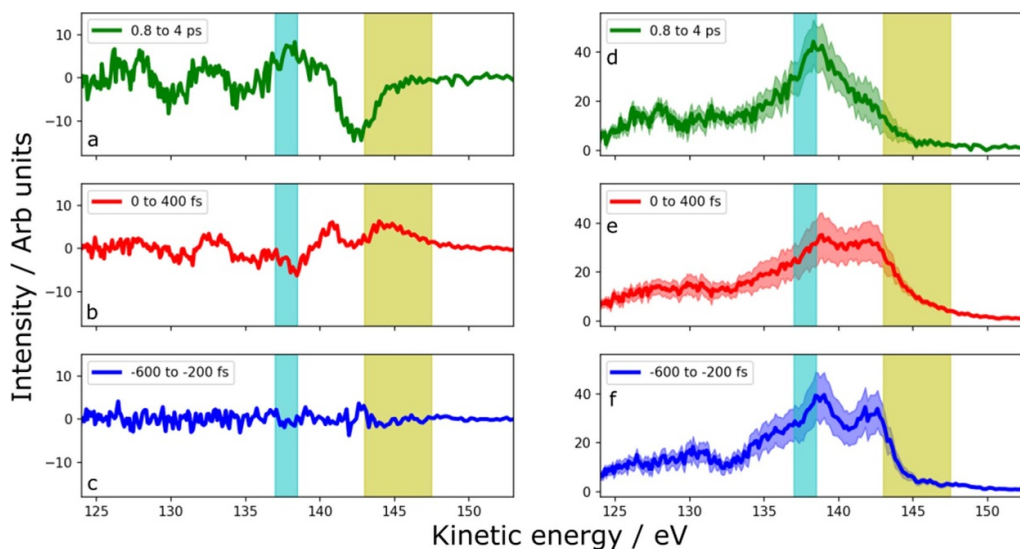


Figure 6. Delay integrated and FEL-only-background subtracted AM spectra. In (a)–(c) the full background is subtracted, which is equivalent to summing over the delay ranges plotted in figure 5. In (d)–(f) the background subtraction is scaled to account for the excited state population. This removes the effect of the ground state depletion and provides an approximate measure of the AM spectrum associated with the ground state of CS₂ (f), the excited states of bound CS₂ (e) and the dissociation products (d). The integrated delay ranges are –600 to –200 fs (c) and (f), 0 to 400 fs (b) and (e) and 0.8 to 4 ps (a) and (d). The shaded regions around the data in panels d–f represent the 3% uncertainty in the excited state population which is used to define the scaling for the background subtraction. The teal and yellow energy regions highlighted show the energy ranges used in the preparation of figure 7.

dissociation products, figure 6(a). The shape of the difference spectrum is however heavily impacted by the overlap with the ground state signal which will also deplete as a consequence of the initial excitation step.

To extract the AM spectrum associated with the integrated delays and remove the impact of the ground state background depletion, we perform a scaled background subtraction of the SLU-FEL spectra which is presented in figures 6(d)–(f). The scaled background subtraction is achieved by subtracting a proportion of the FEL only background from the SLU plus FEL spectrum. The appropriate scaling is obtained via analysis of the depletion seen in the valence region of the spectrum as previously demonstrated in Warne *et al* (2021). This method provided a scaling factor of 0.88 ± 0.03 indicating an excited state population of approximately $12 \pm 3\%$. The spectra obtained from the scaled subtraction are plotted in figures 6(d)–(f) which are integrated over the same time ranges as plots a–c. The shaded region around each spectrum (figures 6(d)–(f)) provides a measure of the error associated with the 3% uncertainty in the excited state population used in defining the background scaling factor.

The signal seen in the early time background subtracted spectrum, figure 6(b), can therefore be rationalised based on the scaled subtraction data. Relative to the ground state spectrum, figure 6(f), the spectrum associated with the excited state, figure 6(e), is skewed and shifted towards higher kinetic energies. From a qualitative picture of the AM decay this might be expected. UV excitation reduces the binding energy of the valence electrons, leading to a higher kinetic energy upon release via AM decay. In an attempt to quantify the energy shift we note that the point at which the

intensity reaches half its maximum value on the higher kinetic energy wing of the peak has increased by approximately 1 eV upon UV excitation. We highlight here that this is simply a qualitative comparison as the excited spectrum has a long tail that extends to much higher kinetic energies. The shift leads to intensity on the blue edge of the ground state peak at energies above 145 eV, and a reduction in intensity at the red edge, around 139 eV. The double peaked structure seen in the ground state appears washed out in the excited state, presumably due to the many different electronic states that are populated over the time range integrated, and the subsequent increase in the number of AM transitions that will contribute to the measured spectrum. We have attempted to sum over smaller time ranges to see if we can isolate any spectral changes associated with the initially excited states and those populated via IC and ISC processes, but this leads to no apparent change in the spectrum beyond degrading the overall statistics. The peaks seen in the background subtracted spectrum plotted in figure 6(b) are therefore a consequence of the difference in shape of the signals associated with the ground state depletion and the excited state enhancement.

At longer delays, the asymptotic spectrum, figure 6(d), skews to the red (compared to the ground and excited state spectra). The previous enhancement seen at the very highest kinetic energies disappears and there is a general reduction in intensity between 140 and 145 eV. At kinetic energies below 140 eV the intensity is enhanced suggesting the effective binding energy for the release of the AM electrons is higher for the reaction products than in the ground and excited states. This is consistent with the known increase in ionisation potential for the CS and S fragments produced. The lack of discernible peaks in the spectrum means we are unable to

differentiate or isolate peaks associated with any of the fragments individually.

The time-dependent shifts in the spectrum therefore characterise the evolving populations of the ground and excited states, as well as those of the dissociation products formed. Due to the broad peaks obtained in the experiments that are associated with multiple overlapping transitions, we cannot differentiate the character of the excited states or fragments. We therefore chose to describe the time dependent signals using the following simplified kinetic scheme where, due to the limited ability to spectrally resolve individual components, we consider all electronically excited states of bound CS₂ together:



Absorption of a 200 nm photon leads to population transfer to an electronically excited state (CS₂^{*}). The temporal profile of the excitation is characterised by the pump and probe pulse cross-correlation which are imprinted into the spectrum as overlapping depletion of the ground state spectrum, and enhancement of the excited state spectrum. Decay of the excited state signal then occurs with an exponential time constant, λ_{ES}, with the associated formation of the dissociation products. Populations of the three separable states for such a model can be expressed mathematically assuming a Gaussian cross-correlation and first order dissociation kinetics. As we perform the fits on the background subtracted data the three components related to the intensity change observed in the spectrum are associated with CS₂ ground state depletion, I_{GSD}, bound but electronically excited CS₂, I_{ES}, and the CS and S dissociation products formed, I_{DP}, such that

$$I_{\text{GSD}} = -A_0 \left(1 - \text{erf} \left(\frac{\Delta t}{\sqrt{2}\sigma} \right) \right) \quad (1)$$

$$I_{\text{ES}} = A_1 e^{-\lambda_{\text{ES}} \Delta t} e^{\frac{(\sigma \lambda_{\text{ES}})^2}{2}} \left(1 - \text{erf} \left(\frac{\Delta t - \sigma^2 \lambda_{\text{ES}}}{\sqrt{2}\sigma} \right) \right) \quad (2)$$

$$I_{\text{DP}} = A_2 \left[\left(1 - \text{erf} \left(\frac{\Delta t}{\sqrt{2}\sigma} \right) \right) - e^{-\lambda_{\text{ES}} \Delta t} e^{\frac{(\sigma \lambda_{\text{ES}})^2}{2}} \times \left(1 - \text{erf} \left(\frac{\Delta t - \sigma^2 \lambda_{\text{ES}}}{\sqrt{2}\sigma} \right) \right) \right] \quad (3)$$

where A_x denotes the amplitude, σ defines the laser cross-correlation, Δt is the pump-probe delay, and λ_{ES} is the rate constant associated with decay out of the excited states and formation of the dissociation products.

Two regions at either end of the background subtracted AM spectrum are fit based on these equations as they contain maximal contribution from the excited state (143 to 147.5 eV) or the dissociation products (137 to 138.5 eV) with minimal contributions from the other components. For clarity, the two

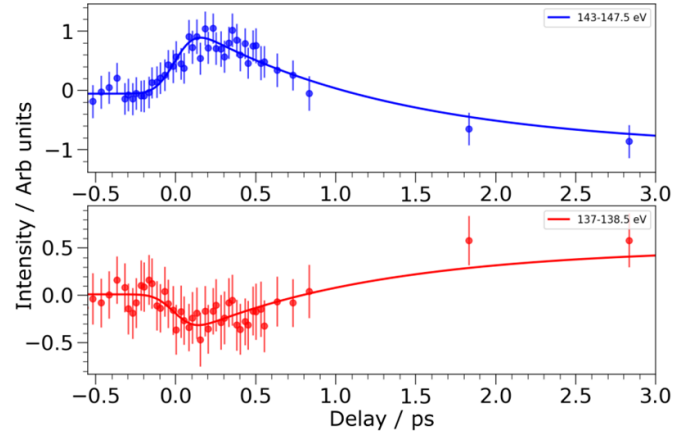


Figure 7. Integrated intensity over the electron kinetic energy range 143–147.5 eV (Top) and 137–138.5 eV (Bottom) and associated fits to equations (4) and (5), respectively. The data point errors represent twice the standard deviation confidence interval obtained through a bootstrap analysis of the integrated photoelectron yields.

energy regions are highlighted in figure 6. The equations fit to these two regions are

$$I_{143-147.5\text{eV}} = I_{\text{ES}} + I_{\text{GSD}} \quad (4)$$

$$I_{137-138.5\text{eV}} = I_{\text{ES}} + I_{\text{DP}} + I_{\text{GSD}}. \quad (5)$$

For $I_{143-147.5\text{eV}}$ the contribution from the dissociation products is minimal and has no impact on the fit, we therefore exclude it here. For the $I_{137-138.5\text{eV}}$ all three components play a role and are included.

The integrated photoelectron yield across these two energy bands and fits to equations (4) and (5) are plotted in figure 7. The fits use the laser cross-correlation and time zero obtained from the valence measurements, providing a σ of 96.1 ± 11.1 fs. This leaves the amplitude A_x and rate constant, λ_{ES}, as the only free parameters in the fit. Both regions are fit independently and return time constants (1/λ_{ES}) values of 1.3 ± 0.2 ps, and 1.2 ± 0.5 ps for $I_{143-147.5\text{eV}}$ and $I_{137-138.5\text{eV}}$ fits, respectively.

As we know, there are two dissociation pathways related to the formation of S(¹D) and S(³P), the simplified kinetic model means the time constant obtained from the fits represents an average dissociation time for the excited states populated. This would include the various singlet and triplet states populated via the various IC and ISC processes that occur. The timescales measured for product formation show strong similarities to the XPS measurements of Gabalski *et al* (2023) where a time constant of 1.2 ps was reported. Both measurements are unable to differentiate the two channels, and as such this timescale provides an effective weighted average of the two pathways.

At earlier times the signal is dominated by the bound excited states of CS₂. The energy shift appears much larger than that seen in the direct XPS spectrum due to the involvement of the valence states in this secondary ionisation process via AM decay. While this provides details of the excited

state lifetime, the complex overlapping nature of the spectrum means it is challenging to extract finer details of the excited state character. The limited spectral resolution attainable with such a spectrometer results in the observed bands being composed of multiple overlapping AM transitions. The resolving power can be improved by means of multi-resolution spectrometers (Viefhaus *et al* 2013, Walter *et al* 2021) at the cost of a drastic reduction in the collection efficiency. The ability to decompose such a spectrum into its constituent parts for a more detailed analysis remains a challenge to experiment and theory alike.

4. Summary

The photodissociation dynamics of CS₂ have been investigated using time-resolved AM spectroscopy at the seeded FEL FERMI in Trieste. The AM spectrum shows time-dependent shifts that correlate with the expected binding energies of the outer valence electron emitted as part of the AM decay such that we observe higher electron kinetic energies for electronically excited states of CS₂, and lower electron kinetic energy for those associated with the CS and S products. How much of the increase in electron kinetic energy associated with the excited states is due to geometric changes (the bending and stretching of the CS bond that leads to a change in the local electronic environment of the S atom) as opposed to electronic (changes in valence character) is currently unknown. At this point it is useful to compare the current results to those previously obtained in the study of two-thiouracil by Lever *et al* (2020). While two-thiouracil is a structurally more complex system, the dynamics are dominated by a single reaction pathway such that the experiments could resolve the systematic shift in peak positions associated with coherent motion out of the Franck–Condon region. In the present work, despite the narrow bandwidth of the FERMI FEL radiation, multiple electronically excited states are populated and the electronic energy levels involved are less easily defined. Thus the range of configurations and AM transitions complicate the spectrum and we do not resolve these changes as clearly.

The experimental capabilities should improve with the development of higher repetition rate FELs in combination with high resolution spectrometers. Systematic studies, by means of TR-AMS while changing the pump wavelength across the barrier to linearity of the excited state, can potentially give information about the different vibrational levels populated and the corresponding change in the nuclear motion of the excited molecular system. In addition TR-AMS, because of its particular sensitivity to reflect the electronic valence structure, can be used in combination with multiphoton or higher photon energy pump pulses to access higher lying valence or Rydberg states.

Time-resolved XPS and AMS are emerging as pump and probe techniques able to investigate the electronic and geometrical structure of molecules. In general TR-XPS is more demanding in terms of photon stability and spectral purity, but

has the advantage of accessing information from an element-specific peak in a region of the photoelectron spectrum that is less congested as compared to TR-AMS. This is particularly beneficial when chemical energy shifts are concerned. On the other hand TR-AMS is well suited for SASE FELs because of its relative insensitivity (at least out of resonances) to the spectral purity of the ionizing radiation. Moreover the increasing use of coincidence techniques at FELs (Kastirke *et al* 2020) is attractive because the information about the two electrons ejected can be collected simultaneously (Hikosaka *et al* 2014). On the theoretical side, the next bottleneck is in developing accurate time-dependent theories that could quantitatively model the expected spectrum for detailed analysis.

Data availability statement

The data that support the findings of this study are available upon reasonable request from the authors.

Acknowledgments

RSM thanks the EPSRC (EP/X027635/1) and Leverhulme Trust (RPG-2021-257) for financial support. HJT thanks the XFEL hub for physical sciences and the University of Southampton for a studentship. RuF and FA gratefully acknowledge support from the Linac Coherent Light Source, SLAC National Accelerator Laboratory, which is supported by the US Department of Energy, Office of Science, Office of Basic Energy Sciences, under Contract No. DE-AC02-76SF00515. RF thanks the Swedish Research Council (Grant Number 2023-03464) and the Knut and Alice Wallenberg Foundation, Sweden (Grant Number 2017.0104). DMPH is grateful to the Science and Technology Facilities Council (United Kingdom) for financial support. MD, DF and CV acknowledge financial support under the National Recovery and Resilience Plan (NRRP), Mission 4, Component 2, Investment 1.1, Call for Tender No. 1409 published on 14.9.2022 by the Italian Ministry of University and Research (MUR), funded by the European Union—NextGenerationEU-Project P20224AWLB “HAPPY” - CUP B53D23025210001 - Grant Assignment Decree No.1386 adopted on 01/09/2023 by the Italian Ministry of University and Research (MUR). D R is supported by the Chemical Sciences, Geosciences, and Biosciences Division, Office of Basic Energy Sciences, Office of Science, U.S. Department of Energy, Grant No. DE-FG02-86ER13491. SC acknowledges support from the Independent Research Fund Denmark-Natural Sciences, DFF-RP2 Grant No. 7014-00258B.

ORCID iDs

Henry J Thompson  <https://orcid.org/0009-0007-2718-2229>

Oksana Plekan  <https://orcid.org/0000-0002-4692-7018>

Nitish Pal  <https://orcid.org/0000-0002-0068-679X>

Felix Allum  <https://orcid.org/0000-0002-8044-8969>
 Alexander D Brynes  <https://orcid.org/0000-0003-2343-7566>
 Piero Decleva  <https://orcid.org/0000-0002-7322-887X>
 Michele Devetta  <https://orcid.org/0000-0002-3806-3475>
 Davide Faccialà  <https://orcid.org/0000-0002-5072-0394>
 Ruaridh Forbes  <https://orcid.org/0000-0003-2097-5991>
 Cesare Grazioli  <https://orcid.org/0000-0002-6255-2041>
 David M P Holland  <https://orcid.org/0000-0003-1351-605X>
 Daniel Rolles  <https://orcid.org/0000-0002-3965-3477>
 Caterina Vozzi  <https://orcid.org/0000-0002-0212-0191>
 Carlo Callegari  <https://orcid.org/0000-0001-5491-7752>
 Russell S Minns  <https://orcid.org/0000-0001-6775-2977>
 Michele Di Fraia  <https://orcid.org/0000-0001-8102-0799>

References

- Allaria E *et al* 2015 *J. Synchrotron Radiat.* **22** 485–91
 Allaria E *et al* 2013 *Nat. Photonics* **7** 913–8
 Ankerhold U, Esser B and von Busch F 1997 *Chem. Phys.* **220** 393–407
 Bisgaard C Z, Clarkin O J, Wu G, Lee A M D, Geßner O, Hayden C C and Stolow A 2009 *Science* **323** 1464–8
 Bolognesi P, O’Keeffe P and Avaldi L 2009 *J. Phys. Chem. A* **113** 15136–41
 Brauße F *et al* 2018 *Phys. Rev. A* **97** 043429
 Brouard M, Campbell E, Cireasa R, Johnsen A and Yuen W H 2012 *J. Chem. Phys.* **136** 044310
 Cinquegrana P, Demidovich A, Kurdi G, Nikolov I, Sigalotti P, Susnjar P and Danailov M B 2021 *High Power Laser Sci. Eng.* **9** E61
 Farmanara P, Stert V and Radloff W 1999 *J. Chem. Phys.* **111** 5338
 Finetti P *et al* 2017 *J. Opt.* **19** 114010
 Gabalski I *et al* 2023 *J. Phys. Chem. Lett.* **14** 7126–33
 Gabalski I *et al* 2022 *J. Chem. Phys.* **157** 164305
 Hedin L, Eland J H D, Karlsson L and Feifel R 2009 *J. Phys. B: At. Mol. Opt. Phys.* **42** 085102
 Hemley R J, Leopold D G, Roebber J L and Vaida V 1983 *J. Chem. Phys.* **79** 5219
 Hikosaka Y, Sawa M, Soejima K and Shigemasa E 2014 *J. Electron Spectrosc. Relat. Phenom.* **192** 69–74
 Hockett P, Bisgaard C Z, Clarkin O J and Stolow A 2011 *Nat. Phys.* **7** 612
 Horio T, Spesyvtsev R, Furumido Y and Suzuki T 2017 *J. Chem. Phys.* **147** 013932
 Horio T, Spesyvtsev R and Suzuki T 2013 *Opt. Express* **21** 22423–8
 Karashima S, Suzuki Y I and Suzuki T 2021 *J. Phys. Chem. Lett.* **12** 3755–61
 Kastirke G *et al* 2020 *Phys. Rev. Lett.* **125** 163201
 Krause M O 1979 *J. Phys. Chem. Ref. Data* **8** 307–27
 Lever F *et al* 2020 *J. Phys. B: At. Mol. Opt. Phys.* **54** 014002
 Lyamayev V *et al* 2013 *J. Phys. B: At. Mol. Opt. Phys.* **46** 164007
 Mank A J G, Starrs C, Jego M and Hepburn J W 1996 *J. Chem. Phys.* **104** 3609–19
 Mayer D *et al* 2022 *Nat. Commun.* **13** 198
 McFarland B K *et al* 2014 *Nat. Commun.* **5** 4235
 Razmus W O *et al* 2022 *Phys. Chem. Chem. Phys.* **24** 15416–27
 Sekushin V, Püttner R, Fink R F, Martins M, Jiang Y H, Aksela H, Aksela S and Kaindl G 2012 *J. Chem. Phys.* **137** 044310
 Smith A D *et al* 2018 *Phys. Rev. Lett.* **120** 183003
 Spesyvtsev R, Horio T, Suzuki Y I and Suzuki T 2015 *J. Chem. Phys.* **142** 074308
 Squibb R *et al* 2018 *Nat. Commun.* **9** 63
 Svetina C *et al* 2015 *J. Synchrotron Radiat.* **22** 538–43
 Townsend D, Satzger H, Ejdrup T, Lee A M D, Stapelfeldt H and Stolow A 2006 *J. Chem. Phys.* **125** 234302
 Unwin J *et al* 2023 *Commun. Phys.* **6** 309
 Viefhaus J, Scholz F, Deinert S, Glaser L, Ilchen M, Seltmann J, Walter P and Siewert F 2013 *Nucl. Instrum. Methods Phys. Res. A* **710** 151–4
 Waller I and Hepburn J 1987 *J. Chem. Phys.* **87** 3261–8
 Walter P *et al* 2021 *J. Synchrotron Radiat.* **28** 1364–76
 Warne E M, Smith A D, Horke D A, Springate E, Jones A J H, Cacho C, Chapman R T and Minns R S 2021 *J. Chem. Phys.* **154** 034302
 Wolf T J A *et al* 2021 *Faraday Discuss.* **228** 555–70